Bioethanol lignin-rich residue from olive stones for electrospun nanostructures development and castor oil structuring

José F. Rubio-Valle, José E. Martín-Alfonso, María E. Eugenio, David Ibarra, José M. Oliva, Paloma Manzanares, C. Valencia

PII: S0141-8130(23)04941-3

DOI: https://doi.org/10.1016/j.ijbiomac.2023.128042

Reference: BIOMAC 128042

To appear in: *International Journal of Biological Macromolecules*

Received date: 19 July 2023

Revised date: 14 October 2023

Accepted date: 9 November 2023

Please cite this article as: J.F. Rubio-Valle, J.E. Martín-Alfonso, M.E. Eugenio, et al., Bioethanol lignin-rich residue from olive stones for electrospun nanostructures development and castor oil structuring, *International Journal of Biological Macromolecules* (2023), https://doi.org/10.1016/j.ijbiomac.2023.128042

Bioethanol lignin-rich residue from olive stones for electrospun nanostructures development and castor oil structuring

José F. Rubio-Valle[a], José E. Martín-Alfonso[a], María E. Eugenio[b], David Ibarra[b], José M. Oliva[c], Paloma Manzanares[c] , C. Valencia[a*]

[a]Pro^{2}Tec*S* – Chemical Product and Process Technology Research Center. Department of Chemical Engineering and Materials Science. Universidad de Huelva. ETSI. Campus de "El Carmen", Huelva 21071, Spain

[b]Instituto de Ciencias Forestales (ICIFOR-INIA, CSIC), Ctra de la Coruña Km 7.5, Madrid 28040, Spain

[c]Biofuels Unit, Renewable Energies Division, CIEMAT. Avda. Complutense 40, Madrid 28040, Spain

* Author to whom correspondence should be addressed:

Prof. C. Valencia, Pro^{2}Tec*S* – Chemical Product and Process Technology Research Center. Dept. Chemical Engineering and Materials Science. ETSI. Campus de "El Carmen", Universidad de Huelva. Huelva 21071, Spain

Phone: +34959218201, e-mail: barragan@uhu.es

Abstract

This work describes the chemical and structural characterization of a lignin-rich residue from the bioethanol production of olive stones and its use for nanostructures development by electrospinning and castor oil structuring. The olive stones were treated by sequential acid/steam explosion pretreatment, further pre-saccharification using a hydrolytic enzyme, and simultaneous saccharification and fermentation (PSSF). The chemical composition of olive stone lignin-rich residue (OSL) was evaluated by standard analytical methods, showing a high lignin content (81.3 %). Moreover, the structural properties were determined by Fourier transform infrared spectroscopy, nuclear magnetic resonance, and size exclusion chromatography. OSL showed a predominance of β-β´ resinol, followed by β-O-4´ alkyl aryl ethers and β-5´ phenylcoumaran substructures, high molecular weight, and low S/G ratio. Subsequently, electrospun nanostructures were obtained from solutions containing 20 wt.% OSL and cellulose triacetate with variable weight ratios in N, N-dimethylformamide/Acetone blends and characterized by scanning electron microscopy. Their morphologies were highly dependent on the rheological properties of polymeric solutions. Gel-like dispersions can be obtained by dispersing the electrospun OSL/CT bead nanofibers and uniform nanofiber mats in castor oil. The rheological properties were influenced by the membrane concentration and the OSL:CT weight ratio, as well as the morphology of the electrospun nanostructures.

Keywords: lignin, olive stones, cellulose triacetate, electrospinning, gel-like dispersion, rheology

1. Introduction

Lignocellulosic biomass (LB) can be transformed into fuels and value-added products in a biorefinery approach [1]. This new production model is a sustainable way to diminish our dependence on fossil fuels and mitigate global warming, based on the abundance, wide distribution, low cost, and non-competition with food of LB to be used as alternative feedstock [2]. Among the lignocellulosic sources that could be employed in a lignocellulosic biorefinery, olive stones (OS), a lignocellulosic by-product of the olive oil industry, can be contemplated as a suitable raw material. They are an abundant material in olive oil-producing countries such as Spain, where the production amounted to around 7.5 million tonnes in 2021 [3]. Taking into account that OS are around 10 % of the olive weight, the amount of these residues generated per year is approximately 750,000 tonnes. OS are removed from the olive fruit in the olive plant, the olive-oil pomace facility, or in both, depending on the local process operation. This residue has been usually used as fuel in small industries and domestic boilers in a changing situation that depends on the energy market conditions and the environmental regulations for its use as a solid fuel [4]. Thus, the valorization of OS in the context of lignocellulosic biorefineries would be of great interest to provide an alternative use for this by-product.

OS have been studied as promising raw material for the production of sugars to obtain advanced biofuels such as bioethanol and further value-added compounds such as xylitol and furfural [5]. The significance of the utilization of lignocellulosic residues to produce bioethanol is currently strengthened by the objectives of the updated Renewable Energy Directive of the European Commission [6]. Among the technologies developed so far to produce bioethanol from LB, the biochemical pathway represents the most favourable [7]. Briefly, this technology involves the release of the fermentable sugars contained in the biomass in the form of carbohydrates (cellulose and hemicellulose) after a pretreatment followed by an enzymatic hydrolysis step and a subsequent step of fermentation to ethanol [1]. Together with ethanol as

the main product, a lignin-rich residue is generated in this process, which in most cases is used as a solid fuel in the facility to produce heat and electricity for the process itself [8]. Lignin is a complex polymeric structure that results from the oxidative coupling of guaiacyl (G) (from coniferyl alcohol), p-hydroxyphenyl (H) (from p-coumaryl alcohol), and syringyl (S) (from sinapyl alcohol) phenylpropane units, producing carbon-carbon and aryl ether chemical bonds [9]. The high carbon content and aromatic structure of lignin, among others, make this lignocellulosic component an interesting raw material for high value-added chemicals and materials production [10], thereby increasing the competitiveness and sustainability of bioethanol production.

One possible way to revalorize these lignin-rich residues is to use them as a thickening or structuring agent of castor oil to produce gel-like dispersions. This is justified as a new way of revalorization and is in line with the new strategic routes that are based on the production of renewable biological resources and the conversion of these resources into high-value-added products [11,12]. In previous research, we have developed environmentally friendly gel-like dispersions in an attempt to imitate the functional properties of conventional lubricating greases [13–15]. Then, growing environmental awareness has led to the substitution of petroleum-based components with renewable materials. For instance, the lubricant industry is not only substituting conventional mineral oils with vegetable oils or glycerol esters [16,17] but also chasing the development of lubricating greases obtained by using environmentally friendly oil structuring and thickening agents to replace metallic soaps, lithium soaps, mainly, with specific rheological properties. Therefore, new oil structuring agents based on renewable materials are needed to solve the existing technical and environmental requirements. Among the different biopolymers studied as oil thickening agents, lignin stands out as a promising alternative after chemical modifications such as functionalization with isocyanates [18,19], acetyl [15] or epoxy [20,21] groups promoting the formation of physical or chemical gels by generating covalent

bonds between the hydroxyl groups of lignin and the vegetable oil. However, although these final formulations may be inert and non-toxic, their processing involves the use of non-environmentally friendly chemicals and solvents. The main difficulty in this regard is to select and develop suitable processing and/or pretreatment protocols for the biopolymer that facilitate efficient interaction with the vegetable oil. A possible solution to overcome this difficulty is to obtain lignin-rich residues-based nanostructures. They present a high porosity and a high area-to-volume ratio that can lead to the development of a three-dimensional network with an outstanding ability to enhance the physical interactions of the thickening agent and the vegetable oil [22–24]. In this regard, electrospinning is one of the most important and widely used techniques for nanofabrication [25], due to the demand for materials with nanoscale dimensions. Thus, it becomes one of the most attractive processes thanks to the ability to transform a wide range of materials into nanostructures at a low cost and with relative simplicity. Several authors have studied the electrospinning process employing lignocellulosic materials [26,27]. It is worth mentioning the studies of Dallmeyer et al. [28,29], Borrego et al. [24,27] and García-Fuentevilla et al. [30,31], where a second polymer is used as a dopant because lignin alone does not create enough entanglements of the polymeric chains within the solution and, therefore cannot generate micro and/or nanometric fibers size. In this sense, the use of cellulose derivatives as a co-spinning polymer stands out due to they generate fibers with relative ease and with properties such as its biocompatibility and high crystallinity, in addition to come from a renewable resource [32–34].

This work investigates the valorization of a lignin-rich residue from bioethanol production of olive stones as a structuring agent of castor oil, through the development of nanostructures with cellulose triacetate in an electrospinning process (Figure 1). The chemical structure of this residue was determined by means of ^{1}H and ^{13}C nuclear magnetic resonance (NMR), two-dimensional NMR (2D NMR), Fourier-transform infrared (FTIR) spectroscopy

and size exclusion chromatography (SEC). In addition, the chemical composition was evaluated by standardized analytical methods. On the other hand, the nanostructures obtained by the electrospinning process of olive stone lignin-rich residue (OSL)/cellulose triacetate (CT) solutions in a mixture of N,N Dimethylformamide (DMF) and acetone (Ac) were likewise assessed by scanning electron microscopy (SEM). The rheological properties of the derived gel-like dispersions were associated with the morphological features of the electrospun nanostructures.

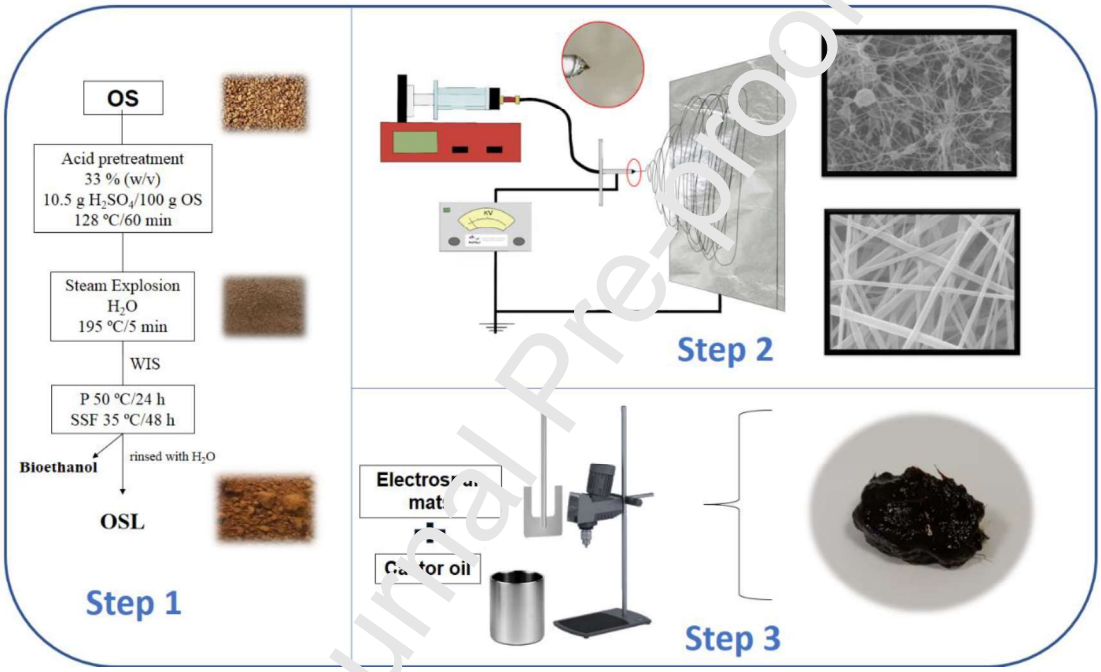

Figure 1. Schematic diagram of the valorization of bioethanol lignin-rich residue from olive stones as a structuring agent for castor oil, by developing nanostructures with cellulose triacetate in an electrospinning process.

2. Materials and Methods

2.1. Raw material and chemicals

Olive stones (OS), with a particle size ranging from 1-3 mm and moisture content of 8%, were supplied by a local company in Jaen (Spain). The material showed the following

chemical composition (dry weight basis): 20.9 % cellulose, 26.0 % hemicelluloses, 35.6 % lignin, 6.3 % extractives, 0.6 % ash, and 5.9 % acetyl groups [5].

Cellulose triacetate (CT) (M_n=100,000 g/mol) was provided by Merck Sigma-Aldrich S.A. (Darmstadt, Germany) and used as a dopant in the polymeric solution to improve the electrospinning process. In addition, N, N-Dimethylformamide (DMF, purity 99.8 %) and acetone (Ac, purity 99.1 %), supplied by Merck Sigma Aldrich S.A. (Darmstadt, Germany) were used as solvents for the preparation of the solutions utilized in electrospinning.

Finally, all other chemicals were reagent-grade and purchased from Panreac (Spain) and Merck Sigma-Aldrich (Darmstadt, Germany). Castor oil from Guinama (Valencia, Spain) was used as an oil medium to prepare gel-like dispersions. The main physical properties and fatty acid composition of castor oil can be found elsewhere [35].

2.2. Production of lignin-rich residue

2.2.1. Pretreatment

OS were subjected to a two-step pretreatment according to Padilla-Rascón et al. [5]. Firstly, an acid pretreatment was carried out at 128 ºC with a solid/liquid ratio of 33 % (wt/v) and 10.5 g H_2SO_4/100 g OS for 60 min in an autoclave. Secondly, a steam explosion pretreatment was performed at 195 ºC for 5 min, using the solid fraction obtained in the acid pretreatment as feedstock. After that, the resulting two-step-pretreated material was filtered and the water-insoluble fraction (WIS) obtained was used as a substrate for bioethanol production in a Simultaneous Saccharification and Fermentation (SSF) process. The chemical composition of the WIS fraction was (dry weight basis): 35.4 % cellulose, 2.6 % hemicellulose, and 57.5 % lignin, determined according to the Laboratory Analytical Procedures for biomass analysis from the National Renewable Energies Laboratory [36], as described below in point 2.2.3.

179 *2.2.2. Simultaneous Saccharification and Fermentation Process (SSF)*

180 SSF was carried out in a two-step procedure. The first step consisted of a
181 presaccharification of the WIS fraction at 20 % (wt/wt) concentration in sodium citrate buffer
182 0.05 M at pH 4.8) in a Terrafors-IS bioreactor 15 L capacity (Infors HT, Switzerland) at 50 ºC
183 for 24 h (final amount of material introduced in the bioreactor was 1.5 Kg). An enzyme dose of
184 30 FPU/g of a dry substrate of Cellic® CTec2 (Novozymes A/S, Bagsværd, Denmark) was
185 used. After the presaccharification step, 0.5 Kg of the incubated materials was transferred to 1
186 L Erlenmeyer flasks to undergo the fermentation stage in an orbital shaker at 150 rpm for 48 h.
187 The temperature was set at 35 ºC, and 1 g/L of *Saccharomyces cerevisiae* ("Ethanol Red",
188 Fermentis, France) of yeast was added with appropriate nutrients, which turned the process into
189 SSF. Experiments were carried out in triplicate. After the fermentation time, the broth was
190 filtered and the insoluble solids were rinsed with abundant water and used as lignin-rich residue
191 (denoted hereinafter as olive stone lignin rich residue (OSL)).
192
193 *2.2.3. Chemical and structural characterization of lignin-rich residue*
194 The chemical composition of OSL was analyzed according to the Laboratory Analytical
195 Procedures for biomass analysis from the National Renewable Energies Laboratory [36].
196 Following this methodology, after the acid hydrolysis of OSL, the acid-insoluble solid residue
197 (Klason lignin) was recovered and weighted, whereas the liquid fraction that contains the
198 monomeric sugars released from the remaining carbohydrates in OSL was analyzed by high-
199 performance liquid chromatography (1260 HPLC, Agilent, Germany, equipped with a G1362A
200 refractive index (RI) detector and an Agilent Hi-PlexPb column) [37]. Acid-soluble lignin
201 content was also measured in the same liquid fraction by UV-Vis spectroscopy.
202 Fourier-transform infrared (FTIR) spectroscopy analysis was performed using a JASCO
203 FT/IR-4200 (Jasco Inc., Japan) apparatus. OSL was dispersed in KBr to obtain disks that were

put in a sample holder. The spectra were collected in a wavenumber range of 400–4000 cm^{-1}, in the transmission mode, at 4 cm^{-1} resolution [18].

^{13}C–^{1}H two-dimensional nuclear magnetic resonance (2D NMR) analysis of OSL (dissolved in 0.75 mL of deuterated dimethylsulfoxide, DMSO-d_6) was recorded at 25 ºC in a Bruker Avance III 500 MHz NMR spectrometer (Billerica, MA, USA). HSQC (heteronuclear single quantum correlation) experiment was recorded according to previously reported operation conditions [18]. Residual DMSO (from DMSO-d6) was used as an internal reference (δ_C/δ_H 39.6/2.5 ppm). The abundance of β-O-4′, β-β′ resinol, β-5′ phenylcoumaran, and spirodienones substructures was estimated from C_α–H_α correlations. Cinnamyl alcohol end-groups using C_γ–H_γ correlations; $C_{2,6}$–$H_{2,6}$ correlations from S units; and C_2–H_2 correlations from G units were used to estimate the S/G lignin ratio.

The total phenols content of OS lignin-rich residue was measured using the Folin-Ciocalteau method modified according to Jiménez-López et al. [37].

Size exclusion chromatography (SEC) analysis of OSL was performed by HPLC (1260 HPLC, Agilent, Germany); fitted with a G1315D diode array detector; and equipped with two columns (Phenomenex) coupled in series (GPC P4000 and P5000) and a safeguard column. The sample (dissolved to a final concentration of 0.5 g /L in NaOH (0.05 M)) was analyzed at 254 nm using NaOH (0.05 M) as a mobile phase pumped at conditions reported by Borrero et al. [18]. Polystyrene sulfonated standards (peak average molecular weights of 4210, 9740, 65,400, 470,000, PSS-Polymer Standards Service) were used for calibration purposes.

2.3. Electrospinning

The electrospun nanostructures were prepared based on previous studies [38]. OSL/CT solutions were manufactured in a DMF/Ac (1:2 v/v) mixture at a 20 wt.% total concentration with variable OSL:CT weight ratios (see Table 1), using a magnetic stirrer (650 rpm) at room

temperature (23 °C) for 24 h. Subsequently, the solutions were placed in centrifuge tubes and centrifuged at 4500 rpm for 7 min to remove the residual impurities.

Table 1. Nomenclature for electrospun OSL/CT nanostructures with different weight ratios

Samples	OSL (%)	CT (%)
OSL100-CT0	100	0
OSL90-CT10	90	10
OSL80-CT20	80	20
OSL70-CT30	70	30
OSL60-CT40	60	40
OSL50-CT50	50	50

The nanofabrication with the OSL/CT solutions was performed in a DOXA Microfluidics (Spain) electrospinning chamber. For this purpose, the syringe was attached to the holder using a horizontal configuration and the high-voltage power supply provided a potential difference of 17 kV. A 21G needle was used and 15 cm was established between the collector plate and the tip of the needle. On the other hand, the OSL/CT solutions were pumped at 0.6 mL/h. All experiments were performed at room temperature (~ 23 ºC) and constant relative humidity (45 ± 1 %).

2.4. Characterization of the OSL/CT solutions

OSL/CT solutions were physicochemically characterized through surface tension, electrical conductivity, and dynamic viscosity measurements. Surface tension measurements were performed on a Sigma 703D tensiometer (Biolin Scientific, Sweden) using a Wilhelmy platinum plate with a measuring range of 1-1000 mN/m. Electrical conductivity was measured in a CE GLP31 conductivity meter (Crison, Spain) at 25ºC, using a conductivity cell previously calibrated with standards of known conductivity. Dynamic viscosity was performed at 25 °C, with a RheoScope (Thermo Fisher Scientific, Waltham, USA) controlled-stress rheometer,

using plate and plate geometry (60 mm diameter, 1 mm gap) in a shear rate range of 1-300 s^{-1}. All measurements were made at least three times.

2.5. Characterization of electrospun OSL/CT nanostructures

The morphological properties of the electrospun nanostructures were determined by scanning electron microscopy (SEM) using a JXA-8200 SuperProbe microscope (JEOL, Japan), with a secondary electron detector at an accelerating voltage of 15 kV. Previously, a sputtering treatment with gold was carried out. An open-source program called DiameterJ was used to analyze the images of the nanostructures.

2.6. Preparation and rheological characterization of the gel-like dispersions from electrospun OSL/CT nanostructures and castor oil

The preparation of the gel-like dispersions from electrospun OSL/CT nanostructures were carried out based on previous studies [23]. The OSL/CT nanostructures obtained during the electrospinning process were carefully removed from the collecting plate with the help of tweezers and a spatula. The electrospun nanostructure (OSL90-CT10) was dispersed with concentrations of 5, 10 and 15 wt.% in castor oil at room temperature (~ 23 ºC) for 24 h, using a controlled-rotational speed mixing device RW 20 from IKA (Staufen, Germany) equipped with an anchor-shaped impeller (75 rpm). In addition, several gel-like dispersions with variable OSL:CT weight ratios (90:10 to 50:50) were prepared at 5 wt.%. in castor oil. The gel-like dispersions were stored at room temperature for further characterization.

Gel-like dispersions were rheologically characterized in a RheoScope (Thermo Fisher Scientific, Waltham, USA) controlled-stress rheometer, using a serrated plate and plate geometry (20 mm diameter, 1 mm gap). Small amplitude oscillatory shear (SAOS) tests were carried out, inside the linear viscoelastic region, in a frequency range of 0.03-100 rad/s at 25

ºC. A stress sweep was previously performed to determine the linear viscoelastic regime. Viscous flow tests were conducted in a shear rate range of 10^{-2}-10^{2} s^{-1} at 25 ºC.

2.7. Statistical Analysis

An analysis of the variance (ANOVA) was performed using three replicates of each measurement independently. Furthermore, a comparison of means tests was performed to detect significant differences ($p < 0.05$).

3. Results and discussion

3.1. Chemical and structural characterization of lignin-rich residue

3.1.1. Chemical characterization

The chemical composition of OSL revealed a rather high lignin content (81.3 % total lignin; 80.6 % of acid-insoluble lignin and 0.7 % of acid-soluble lignin) compared to raw olive stones (35.6 % total lignin). This lignin concentration is due to the significant hydrolysis and solubilisation of hemicelluloses contained in olive stones material by acid pretreatment followed by steam explosion, as well as the glucose release in the subsequent enzymatic hydrolysis of the resulting pretreated material [39,40]. Despite the two-step pretreatment and the SSF, it was still possible to quantify certain carbohydrate content in the OSL, mainly glucan (12.2 %) and to a lesser extent xylan (1.1 %). It is well known that a part of the cellulose contained in LB is recalcitrant to the action of cellulolytic enzymes and that the carbohydrate content found in the residue depends largely on the severity of the pretreatment and the SSF conditions [41] Similar results have been reported in lignin-rich residues generated during bioethanol production from olive tree pruning, including steam explosion or acid catalysed steam explosion as pretreatments and subsequent saccharification and fermentation processes [42,43]. The presence of carbohydrate impurities detected in lignin may have a possible

influence on its valorization way, and based on the requirements of the target application some lignin purification may be necessary. Nonetheless, lignins with certain carbohydrate content have shown a positive effect on their subsequent valorization process as a thickening or structuring agent in vegetable oils by chemical functionalization [18,44].

3.1.2. Structural characterization

The characteristic functional groups of lignin-rich residue were evaluated by FTIR spectroscopy (Figure 2a). As with other lignin-rich residues generated during bioethanol production from olive-based materials, such as olive tree pruning [42,43], the OSL FTIR spectrum contains the typical lignin and carbohydrate bands. Regarding lignin, bands around 1330 cm^{-1}, 1268 cm^{-1} and 833 cm^{-1}, associated with syringyl (S), guaiacyl (G) and *p*-hydroxyphenyl (H) units, respectively were observed, together with bands at 1600 cm^{-1}, 1511 cm^{-1}, and 1422 cm^{-1} attributed to aromatic skeleton lignin vibrations. A wide O–H absorption peak at 3335 cm^{-1} from lignin and carbohydrates was also clearly visible. Finally, two bands attributed to lignin oxidation could also be detected. On one side, a slight absorption at 1700 cm^{-1} was associated with unconjugated C=O groups. Nevertheless, carbonyl groups of hemicelluloses contained in OSL could also be contributing to this absorption [45]. On the other side, conjugated C=O groups at 1647 cm^{-1} could be found, although this band could also be associated with amide bonds from hydrolytic enzymes used during saccharification [46]. Concerning carbohydrates, cellulose and hemicellulose bands at 1156 cm^{-1}, 1116 cm^{-1}, and 1030 cm^{-1} are visible, some of them overlapping lignin bands.

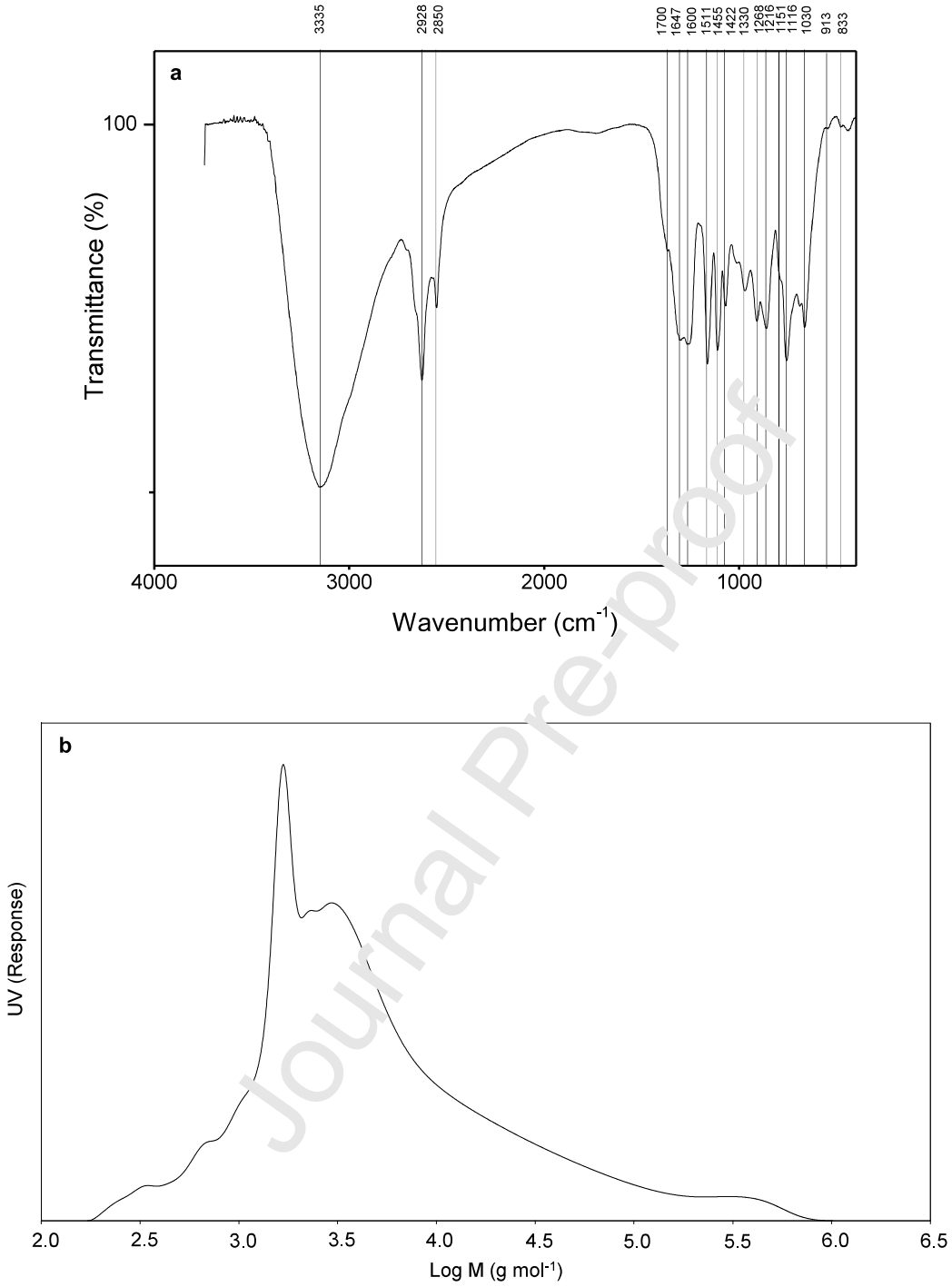

Figure 2. a) FTIR spectrum, 4000-750 cm^{-1}, of olive stone lignin-rich residue and b) the molecular weight distribution of olive stone lignin-rich residue.

The main lignin and carbohydrate substructures were detected by 2D NMR analysis (HSQC spectra are displayed in Figure 3 and recognized substructures in Figure 4). OSL HSQC spectra show the typical lignin and carbohydrate signals (listed in Table 2), which were assigned

according to those described by different published studies on both native lignin and bioethanol lignin-rich residues from olive tree pruning [42,43]. Despite the degradation of β-O-4′ alkyl aryl ethers (A), β-β′ resinol (B) and β-5′ phenylcoumaran (C) native substructures reported by several authors during acid and steam explosion pretreatments of aspen and poplar woody materials as well as during enzymatic hydrolysis [47–49], the aliphatic-oxygenated region of OSL HSQC spectrum still displayed correlation signals of them (Figure 3b). Moreover, possible condensation reactions can also take place during these pretreatments [47,50]. Then, OSL showed a predominance of β-β′ resinol substructures (42.1 % of the total inter-unit linkages), followed by β-O-4′ alkyl aryl ethers (31.4 %), and β-5′ phenylcoumaran substructures (17.3 %). Other native lignin correlation signals were also visible, such as those corresponding to spirodienones (E) and cinnamyl alcohol end-groups (I), with relative percentages of 9.1 % and 1.75 %, respectively.

Table 2 Assignment of main lignin and carbohydrates ^{13}C-^{1}H correlation peaks in the 2D NMR HSQC spectra of olive stone lignin-rich residue

δ_C/δ_H (ppm)	Assignment
54.0/3.04	C_β–H_β, resinol substructures (**B**)
56.1/3.72	C–H, methoxyls (**MeO**)
60.6/3.38–3.64	C_γ–H_γ, β-O-4′ substructures (**A**)
61.9/4.07	C_γ–H_γ, cinnamyl alcohol end groups (**I**)
62.7/3.65	C_γ–H_γ, phenylcoumaran substructures (**C**)
63.2/3.21–3.89	C_5–H_5, xylan
71.3/3.76–4.18	C_γ–H_γ, resinol substructures (**B**)
71.5/4.78	C_α–H_α, β-O-4′ **G** unit (**A**)
72.1/4.87	C_α–H_α, β-O-4′ **S** unit (**A**)
72.7/3.07	C_2–H_2, xylan
74.0/3.26	C_3–H_3, xylan
75.7/3.54	C_4–H_4, xylan
81.6/4.72	C_α–H_α, spirodienone substructures (**E**)
83.8/4.26	C_β–H_β, β-O-4′ **G** unit (**A**)
85.3/4.74	$C_{\alpha'}$–$H_{\alpha'}$, spirodienone substructures (**E**)
85.5/4.63	C_α–H_α, resinol substructures (**B**)
87.5/5.42	C_α–H_α, phenylcoumaran substructures **G** units (**C**)
88.5/5.59	C_α–H_α, phenylcoumaran substructures **S** units (**C**)
92.3/4.89	reducing end (1–4) α-D-Xylp
97.3/4.27	reducing end (1–4) β-D-Xylp
104.3/6.69	$C_{2,6}$–$H_{2,6}$, S units (**S**)
106.2/7.12	$C_{2,6}$–$H_{2,6}$, in cinamaldehyde end-groups **S** units (**J**)

106.7/7.32	$C_{2,6}$–$H_{2,6}$, oxidized (H–C_α=O or H_3C–C_α=O) S units (**S′**)
111.0/6.88	C_2–H_2, G units (**G**)
111.0/7.38	C_2–H_2, oxidized (H–C_α=O) G units (**G′**)
115.0/6.74	$C_{3,5}$–$H_{3,5}$, *p*-hydroxyphenyl (**H**)
115.2/6.42-6.81	C_5–H_5, G units (**G**)
119.4/7.30	C_6–H_6, in cinamaldehyde end-groups **G** units (**J**)
119.6/6.78	C_6–H_6, G units (**G**)
123.6/7.51	C_6–H_6, oxidized (H_3C–C_α=O) G units (**G″**)
128.3/7.19	$C_{2,6}$–$H_{2,6}$, p-hydroxyphenyl (**H**)

Finally, this aliphatic-oxygenated region of OSL also revealed carbohydrate signals (Figure 3b), either from hexose or pentose units, according to the chemical composition determined. These signals comprised mainly correlations of the xylan chain (X), together with the cross peaks for α - and β-xylose reducing ends (Figure 3*a*).

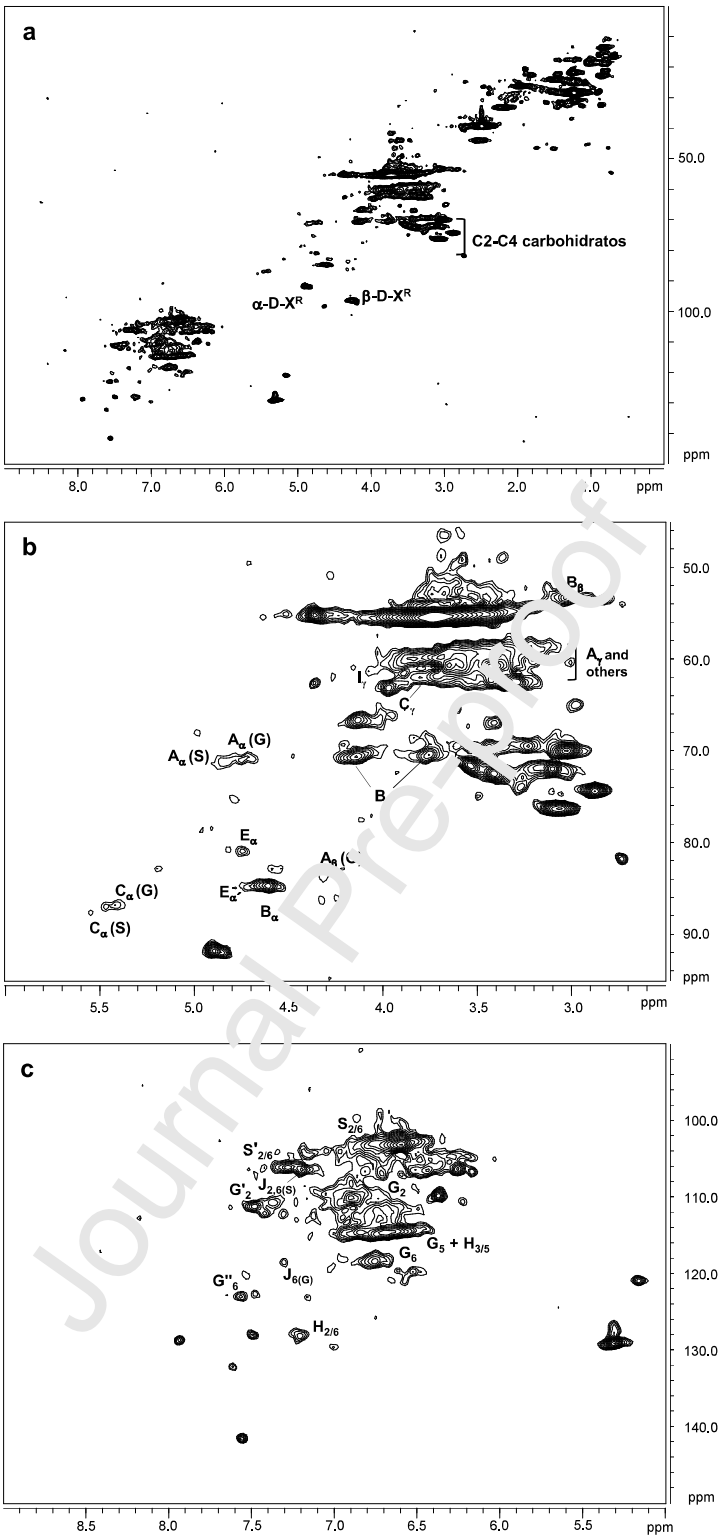

Figure 3. 2D-NMR HSQC spectra of olive stone lignin-rich residue. a) whole spectrum, δ_C/δ_H 0.0–150.0/0.0–9.0 ppm; b) aliphatic oxygenated region, δ_C/δ_H 45.0–95.0/2.5–6.0 ppm; and c) aromatic region, δ_C/δ_H 90.0–150.0/5.0–9.0 ppm.

Regarding the aromatic region of the OSL HSQC spectrum (Figure 3c), the characteristic correlation signals of S, G, and H lignin units were seen, in the same way that FTIR analysis. From them, the S/G ratio calculated was 1.37, slightly higher than native lignin from olive tree pruning [51]. Moreover, several correlation signals corresponding to lignin oxidation could also be found, supporting the observations previously described by FTIR. These signals include those attributed to oxidized S units ($S'_{2,6}$), such as syringaldehyde and acetosyringone, and those corresponding to oxidized G units endorsed to vanillin (G'_2) and acetovanillone (G''_6). On the other hand, signals found at δ_C/δ_H 105.0/6.5, 112.8/6.7, and 119.7/6.5 ppm were tentatively attributed to possible condensation reactions of lignin occurred during acid pretreatment or steam explosion [52]. Nevertheless, these correlation signals have also been associated with gallate and catechol-type structures [53] and most likely belong to condensed tannins consisting of gallocatechin units [54]. The presence of tannins has been recently reported in olive stones [55]. Finally, other native lignin units corresponding to cinnamaldehyde end-groups (J) in S units (sinapaldehyde end-groups) and in G units (coniferaldehyde end-groups), previously described in lignin from olive tree pruning [56,57], could also be identified in lignin from olive stone.

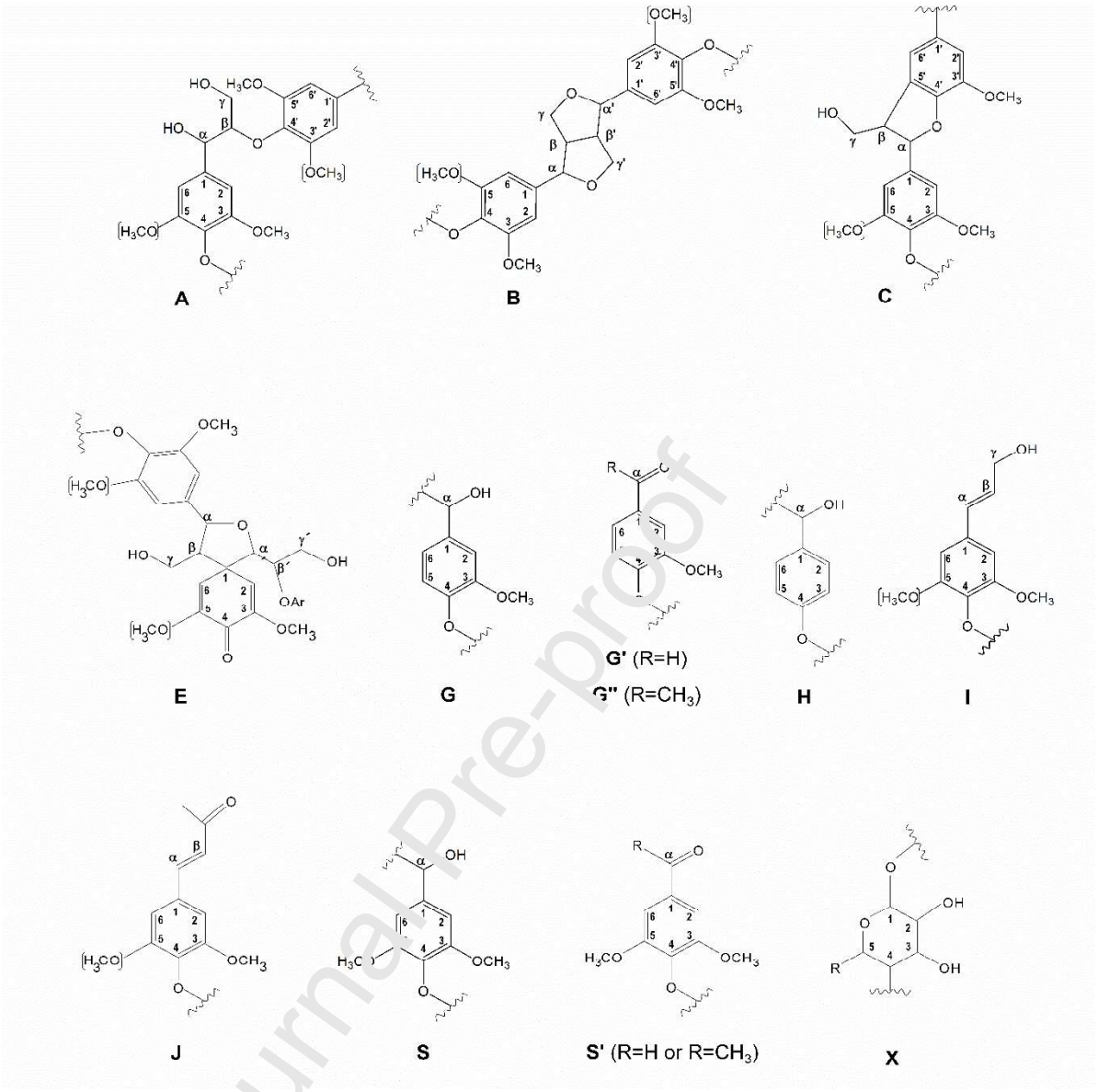

364

365 **Figure 4**. Main lignin and carbohydrate substructures identified in aliphatic oxygenated and
366 aromatic regions of olive stone lignin-rich residue: (A), β-O-4' alkyl-aryl ether; (B), β-β´
367 resinols; (C), β-5´phenylcoumarans; (E), spirodienones; G), guaiacyl unit; (G'), vanillin; (G"),
368 acetovanillona; (H), p-hydroxyphenyl unit; (I), cinnamylalcohol end-groups; (J), cinnamyl
369 aldehyde end-groups; (S), syringyl unit; (S'), syringaldehyde or acetosyringone; (X),
370 xylopyranose (R, OH).

371

372 The molecular weight distribution of OSL is shown in Figure 2b. Several fractions are
373 displayed, including one with a broad peak of higher molecular weight and the other with a

narrow peak of lower molecular weight. Molecular weight and polydispersity values (M_w, 24965 Da; M_n, 2175 Da; PD, 11.4) could be calculated from this molecular weight distribution. These values are similar to those reported for lignins remaining in the insoluble residue from enzymatic hydrolysis of pretreated materials (from eucalypt, pine, and black locust woody materials) [18,58]. The remaining β-O-4′ alkyl aryl ethers substructures after acid and steam explosion pretreatments can contribute to high molecular weight values, in spite of their degradation described during these processes [47], together with possible polymerization reactions, mainly via C–C bonds, which are also produced under these pretreatments [47]. In this sense, the high polydispersity value observed (11.4) could support that polymerization reactions have taken place during both acid and steam explosion pretreatments [59].

3.2. Physicochemical properties of OSL/CT solutions and morphology of electrospun nanostructures.

The skill to produce fibers during the electrospinning process lies in the physicochemical properties of the solutions and the fact that the polymer chains can achieve entanglements, as well as operating parameters (voltage, distance between the tip and collector, flow rate, humidity, and temperature). Some of these key intrinsic properties of the solution itself are dynamic viscosity, surface tension and electrical conductivity, which depend on the type of biopolymer, its concentration [22,27,30], and the solvent [60]. Table 3 displays the dynamic viscosity, surface tension and electrical conductivity values for the solutions prepared at different OSL:CT weight ratios. All the solutions present a Newtonian behavior in the range of the applied shear rate. As can be observed, the dynamic viscosity increases by increasing CT proportion, as previously studied with electrospun solutions of eucalyptus kraft lignin and cellulose acetate [38]. On the other hand, the incorporation of OSL and OSL/CT causes an increase in the surface tension of the DMF:Ac mixture (26.7 mN/m), which could be attributed

399 to an increase in the interaction between the solvent mixture and OSL. This is due to intra- and
400 intermolecular interactions between aromatic rings of lignin in DMF:Ac mixtures [61]. The
401 phenolic nature of OSL detected (the content of 55 ± 2.3 mg GAE/g lignin-rich residue was
402 calculated by Folin-Ciocalteau method) leads to the enhancement of these interactions [62]. In
403 addition, the higher the amount of CT, the higher the surface tension values, because of the
404 hydrophobic character of CT. On the other hand, the electrical conductivity value of the solvent
405 blend was 3.2 μS/cm, so the addition of OSL causes a similar effect to that presented in the
406 surface tension values, increasing the starting values of the solvent mixture, which could be
407 attributed to an increase in the number of ions due to the polarity presented by OSL [38].
408 However, when the OSL:CT weight ratio was decreased, it caused a decrease in the electrical
409 conductivity, given the lower molecular weight and more polar character of OSL as a
410 consequence of the chemical structure composed of phenolic and aliphatic hydroxyl and
411 carboxyl moieties, as shown above by FTIR and NMR.

412
413 **Table 3.** Dynamic viscosity, surface tension and electrical conductivity values for OSL/CT
414 solutions with different weight ratios

OSL:CT weight ratio	η (mPa.s)	Surface tension (mN/m)	Electrical conductivity (μS/cm)
100:0	3.1^{a}	30.3^{A}	155.6^{aA}
90:10	21.4^{b}	32.1^{B}	135.2^{bB}
80:20	30.1^{b}	33.1^{C}	125.5^{cC}
70:30	55.3^{c}	34.3^{C}	117.8^{cC}
60:40	98.7^{d}	36.1^{D}	101.6^{dD}
50:50	209.7^{e}	37.9^{E}	92.1^{eE}

415 *Note: Values differing in the superscripts are significantly different ($p < 0.05$)*

416

417 Figure 5 shows the micrographs of the different electrospun nanostructures obtained by
418 SEM from the solutions prepared with variable weight ratios of OSL:CT. As can be observed,
419 the electrospinning of the solution without CT in the composition did not generate nanofibers,

but, on the contrary, the resulting nanostructures consisted of micrometer-sized particles, which are distributed forming agglomerates (Figure 5a). On the one hand, the microstructures of the solutions in which a lower amount of CT has been added (Figure 5b and 5c), presented nanometric fibers and particles, where fibers are intertwined with each other, and particles are interconnected. On the other hand, increasing the proportion of CT in the solution resulted in higher density and greater fiber abundance, as well as a slightly larger size of them (Figure 5d). Finally, in the micrographs of the systems in which 60:40 and 50:50 OSL:CT were used (Figure 5e and 5f), it is observed that there are practically no OSL nanoparticles in the nanostructures, but they are integrated into the fibers themselves, forming a homogeneous structure. These results are because the increase of CT proportion in the solution causes an increase in the amount of entanglement of the polymer chains, due to the higher viscosity of the solution, as mentioned above. Moreover, these results agree with those obtained by other authors [27,28,38], showing the need for a second linear and high-molecular-weight polymer to act as a dopant given the inability of OSL to form entanglements between their polymer chains to generate fibers during the electrospinning process.

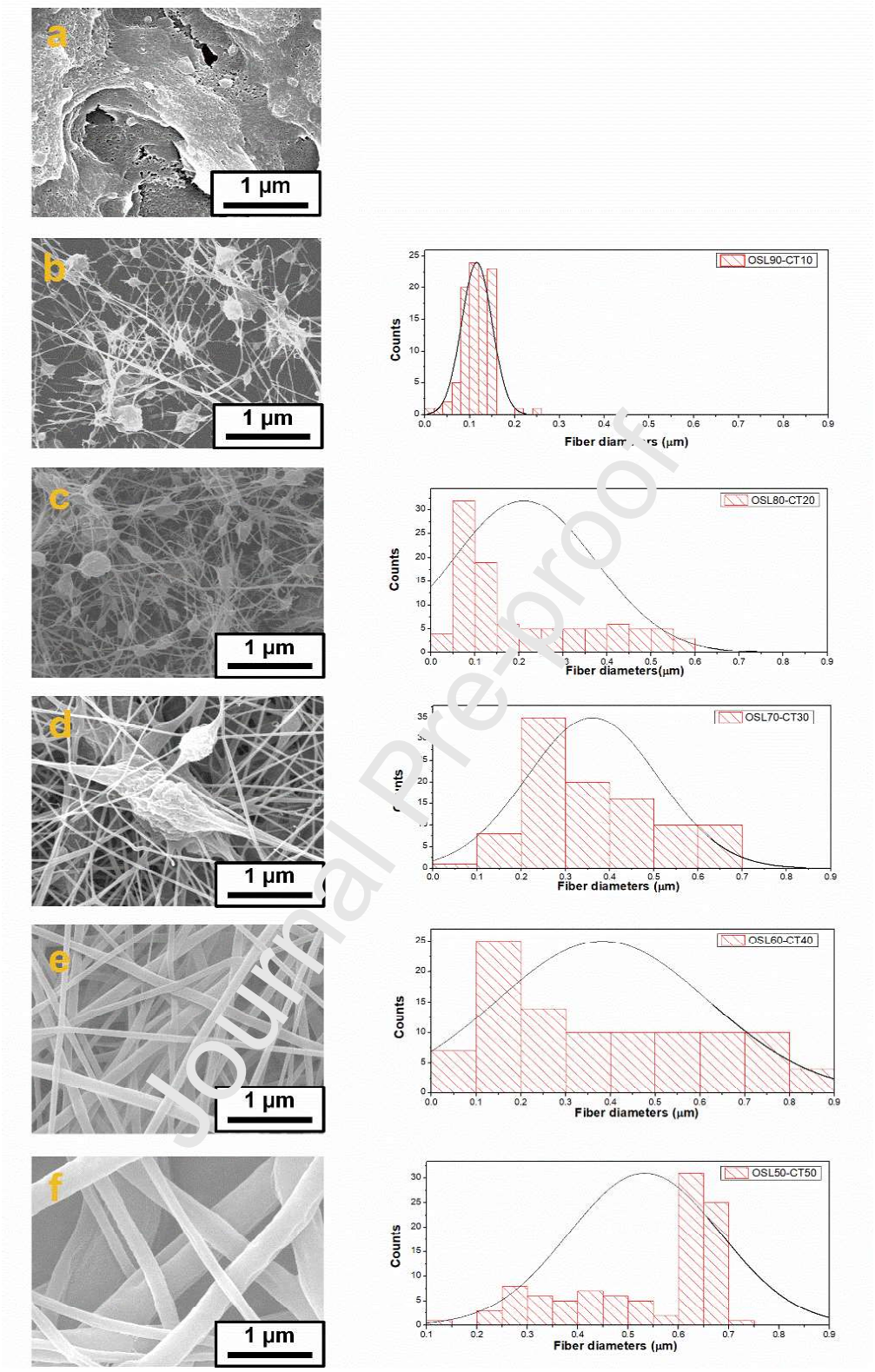

436

437 **Figure 5.** SEM images of electrospun nanostructures obtained from solutions with variable
438 OSL:CT weight ratios and fiber size distribution. a) OSL100-CT0, b) OSL90-CT10 c) OSL80-
439 CT20, d) OSL70-CT30 d) OSL60-CT40, f) OSL50-CT50.

The fiber size distribution and a Gaussian fit, which allows to obtain the average fiber size of the electrospun nanostructures generated during the electrospinning process, can also be observed in Figure 5. These distributions support the findings obtained from the micrographs, i.e., a significant increase in the average diameter of the fibers is obtained by increasing CT proportion. On the other hand, all the histograms of fiber diameter present a heterogeneous multidisperse distribution, except for the OSL90-CT10 system, which displays a homogeneous and monodisperse distribution as a consequence of the fact that the fibers intertwine the nanoparticles and these are not integrated into the fibers themselves, as occurs by increasing CT proportion.

Table 4 lists the average diameters of particles and fibers calculated from the size distributions of the electrospun nanostructures. As can be seen, there is a decrease in the mean particle size by increasing the CT proportion, because the particles are integrated into the fibers themselves. On the contrary, regarding the diameter of fibers, it is observed that the increase in the CT proportion leads to an increase in the average particle size. On the other hand, it is well known that an adequate electrospinnability of polymeric solutions can be accomplished with proper physicochemical properties (electrical conductivity, surface tension and dynamic viscosity) of the solution. Thus, by decreasing surface tension and increasing conductivity the jet formation and stretching of the nanofibers is facilitated, while high viscosity retards stretching, but prevents filament breakage then increasing fiber diameter [23,38]. Therefore, the lower the OSL:CT weight ratio, the higher the viscosity of the solution, favors an increase in fiber diameter. On the contrary, the higher the content of OSL, the higher the electrical conductivity and the lower the surface tension, which favors the thinning of the filaments and/or their rupture, essentially resulting in the formation of particles**.** These results are consistent with a previous work [38], where the electrospinning process of eucalyptus Kraft lignin and cellulose acetate solutions was studied.

Table 4. Average particle and fiber diameters of the OSL/CT electrospun nanostructures

Sample Code	Average particle diameter (μm)	Average fiber diameter (μm)
OSL100-CT0	4.1	-
OSL90-CT10	1.7	0.12
OSL80-CT20	0.9	0.21
OSL70-CT30	0.6	0.34
OSL60-CT40	0.4	0.39
OSL50-CT50	-	0.52

3.3. Castor oil structuring ability of electrospun OSL/CT nanostructures

Several studies have already reported the production of gel-like dispersions employing electrospun mats as a thickening agent in castor oil [22,60]. Borrego et al. [24] and Rubio-Valle et al. [23,38] studied the ability to structure castor oil incorporating electrospun low-sulfonate Kraft lignin/polyvinylpyrrolidone and eucalyptus Kraft lignin/cellulose acetate nanostructures, respectively. The authors highlight that electrospun mats consisting only of micro or nanometer-sized particles lead to the separation of the nanostructure from the castor oil over time, because of weak interactions with the oil. On the other hand, electrospun mats formed by micro or nanosized fibers result in stable gel-like dispersions due to physical interactions, mainly intermolecular hydrophobic and Van der Waals forces, resulting from high surface area/volume ratio of the nanofibers [38].

The electrospun nanostructure obtained from the OSL90-CT10 solution was dispersed in castor oil with concentrations of 5, 10, and 15 wt.%, at room temperature, and the rheological response was analysed. Figure 6a depicts the mechanical spectra of the resulting gel-like dispersions, in the linear viscoelasticity range, as a function of the electrospun mats concentration. The evolution of the storage, G', and loss, G" moduli, with the frequency, is characteristic of gel-like dispersions [63,64] and qualitatively similar to the three electrospun mat concentrations, being G' always higher than G" in the whole frequency range studied. In addition, a plateau region can be noticed at low and intermediate frequencies, while at high

485 frequencies a tendency to reach a crossing point between both moduli can be observed. Anyway,
486 the higher the electrospun mats concentration, the higher the viscoelastic functions, indicating
487 a stronger microstructural network. However, the relative elasticity was almost unaffected at
488 low frequencies, as can be seen in Figure 6b, where the plots of the loss tangent (tan δ = G”/G´)
489 versus frequency are shown. Only gel-like dispersions having low thickener concentration (5
490 wt.%) present higher values of the loss tangent at high frequency. As previously described [65],
491 the values of the SAOS functions depend basically on the content by weight of the thickening
492 agent, i.e. the content of the electrospun mats used in the gel-like dispersion. On the other hand,
493 to study the effect of the electrospun mats OSL:CT weight ratio on linear viscoelasticity and
494 viscous flow, a concentration of 5 wt.% was selected.

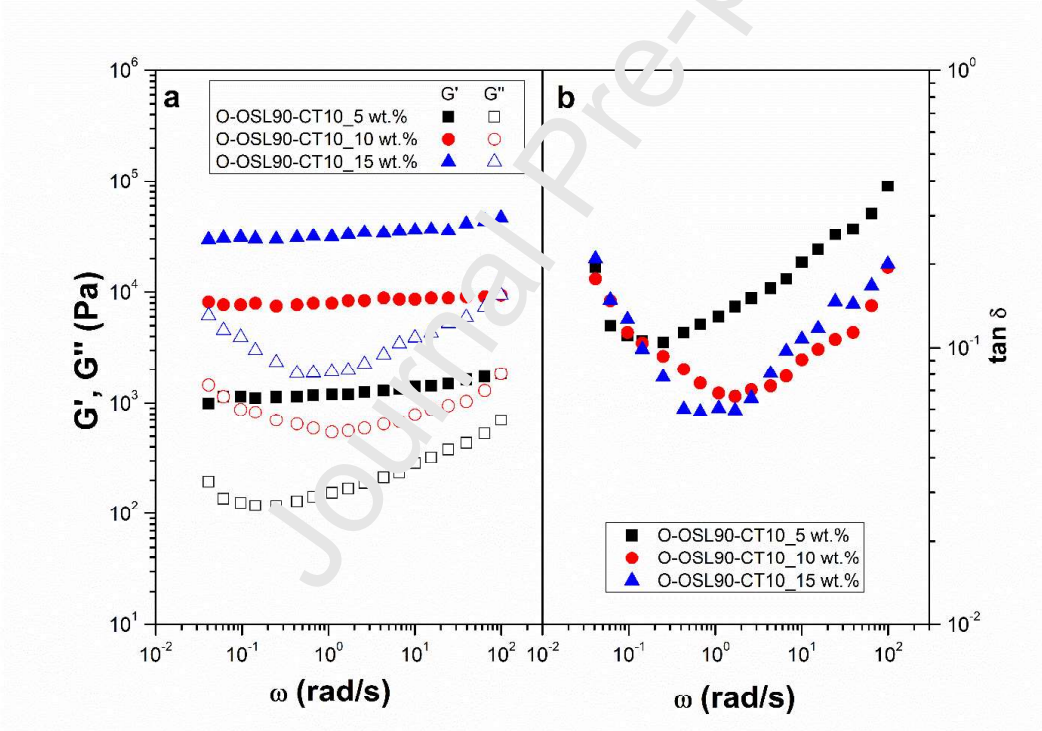

495

496 **Figure 6.** Frequency dependence of a) the storage (*G*) and loss (*G*) moduli and b) the
497 loss tangent, for gel-like dispersions prepared with the OSL90-CT10 nanostructure at 5, 10
498 and 15 wt.%.

499 Figure 7 illustrates the variation of the SAOS functions (viz., the storage modulus, G′
500 and loss modulus, G″) with frequency for gel-like dispersions prepared with variable

electrospun OSL:CT weight ratio (90:10 to 50:50). As can be seen, the SAOS functions frequency dependence is not qualitatively influenced by the electrospun OSL:CT nanostructure weight ratio in the frequency range studied. However, G' and G'' increased markedly by decreasing OSL:CT weight ratio due to an increased proportion of the component with the higher average molecular weight (CT) in the nanostructure and morphological properties (higher average fiber). On the other hand, relative elasticity increases as the proportion of CT increases (Figure 7c). It should be noted that with an electrospun mats concentration of 5 wt.% and OSL:CT weight ratio of 90:10, 80:20 and 70:30 or 5, 10 and 15 wt % concentration and 90:10 weight ratio is possible to obtain values of the viscoelastic functions comparable to those exhibited by conventional lubricating greases, with typical G' values of 10^3-10^5 Pa depending on the thickener and concentration, and G'' values around one order of magnitude lower [66,67]. Furthermore, these results are in agreement with those of other studies in which an increase in the dopant biopolymer proportion leads to an increase in SAOS functions [22,60]. On the other hand, Borrego et al [27] and Rubio-Valle et al [38] obtained similar values of viscoelastic functions but at higher concentrations of thickener, developing electrospun low-sulfonate lignin/polyvinylpyrrolidone and eucalyptus Kraft lignin/cellulose acetate nanostructures, respectively, to structure castor oil.

In order to demonstrate the above-mentioned effect of electrospun nanostructure morphology on the viscoelastic response of gel-like dispersions, the plateau modulus (G_N^0), as defined elsewhere [68], is plotted in Figure 7d as a function of mean fiber diameter, showing a power-law evolution with this parameter.

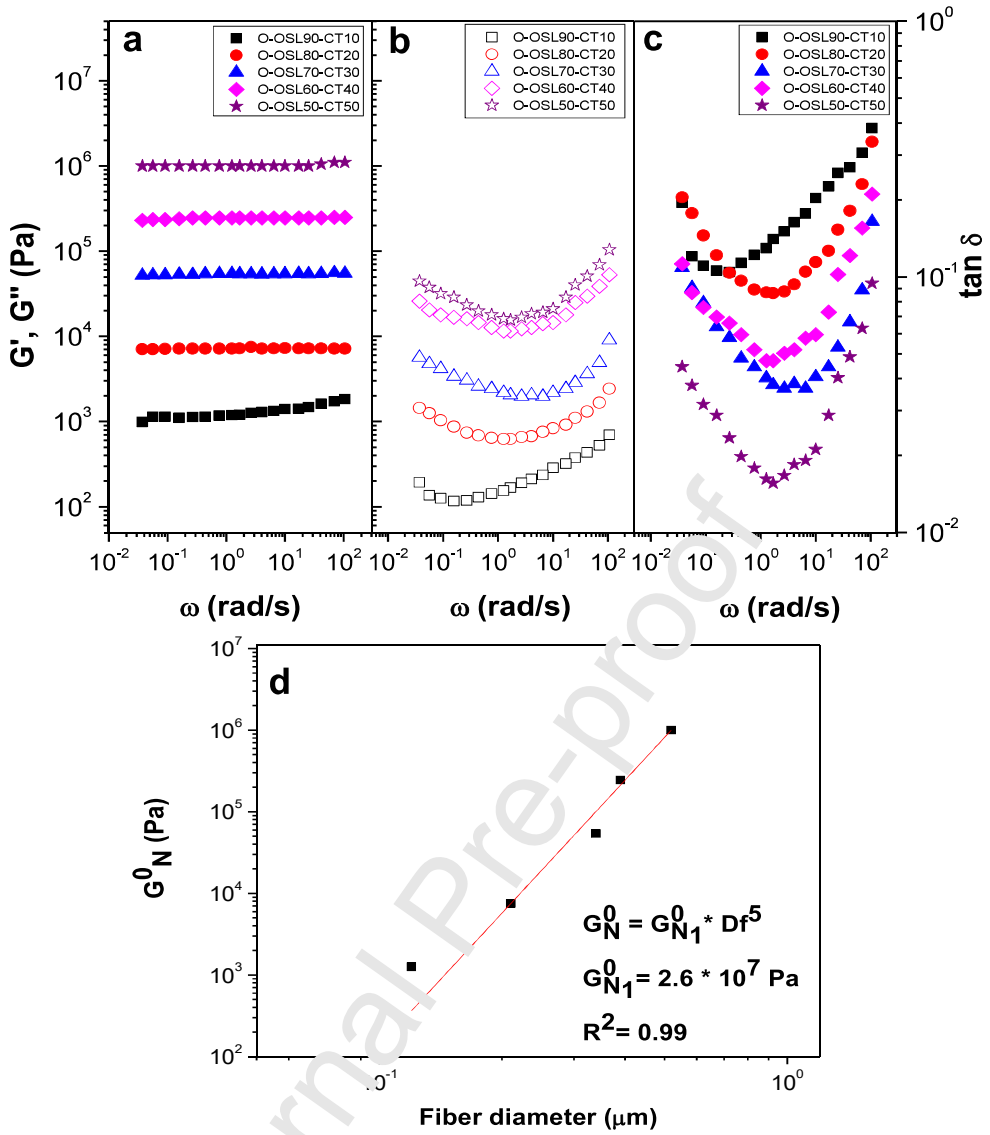

522

523 **Figure 7.** Frequency dependence of a) the storage modulus, G', b) the loss modulus, G'', c)

524 the loss tangent, for gel-like dispersion prepared with variable OSL:CT weight ratio at 5 wt.%

525 and d) dependence of the plateau modulus with fiber diameter of nanostructure, for gel-like

526 dispersions prepared with variable OSL:CT weight ratio.

527 On the other hand, Figure 8a displays the viscous flow curves of OSL/CT nanofiber

528 structured gel-like dispersions as a function of the OSL:CT weight ratio. The power law model

529 adequately fits the shear thinning behavior:

530 $$\eta = K \cdot \dot{\gamma}^{\,n-1} \qquad \text{(eq 1)}$$

531 where K and n are the consistency and the flow indexes, respectively.

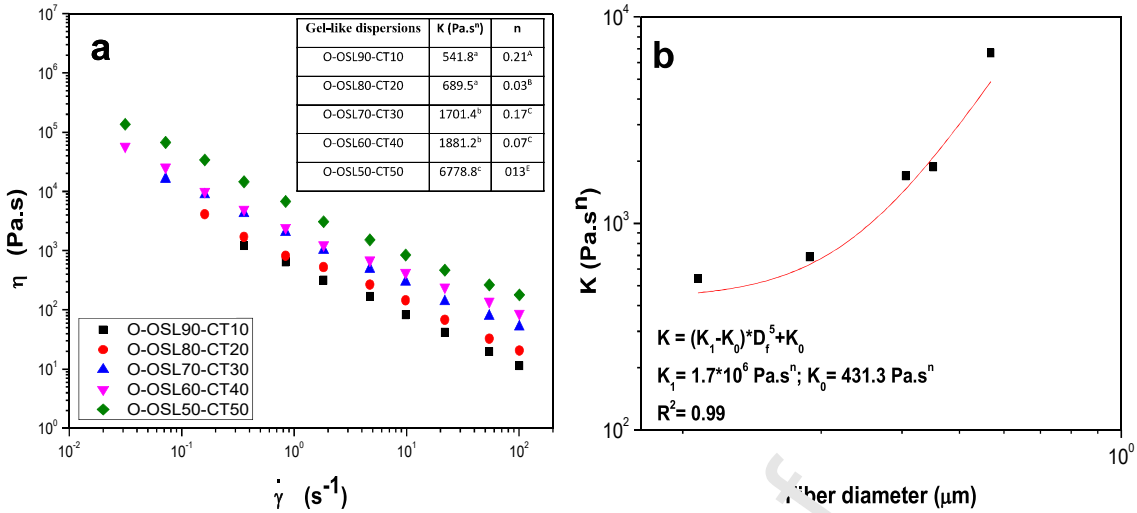

532

533 **Figure 8.** a) Viscous flow curves and b) dependence of the consistency index (K) with

534 average fiber diameter for gel-like dispersions prepared with variable OSL:CT weight ratio.

535

536 The Table inside Figure 8a provides the values of both fitting parameters for the

537 different gel-like dispersions. Similarly to SAOS functions, K increased by decreasing OSL:CT

538 weight ratio and depends on the morphological properties of the electrospun OSL/CT

539 nanostructures. On the other hand, the low values of the flow index, n, reveal a shear-thinning

540 response, which is typical of materials with markedly non-Newtonian properties such as

541 conventional lubricating greases [67]. Figure 8b illustrates the relationship between K and the

542 mean fiber diameter and as can be seen, K potentially evolves with this parameter.

543

544 **4. Conclusions**

545 Olive stones (OS) were submitted to a sequential acid/steam explosion

546 pretreatment,which was followed by a presaccharification, saccharification and simultaneous

547 saccharification and fermentation (PSSF) process of the pretreated material to obtain a liquid

548 media containing ethanol and a lignin-rich solid residue . This resulting OS lignin-rich residue

549 (OSL) displayed high lignin content along with some carbohydrate impurities. In addition, OSL

showed a predominance of β-β′ resinol substructures (42.1 % of the total inter-unit linkages), followed by β-O-4′ alkyl aryl ethers (31.4 %), and β-5′ phenylcoumaran substructures (17.3 %), together with high molecular weight, and low S/G ratio and phenolic content. Subsequently, nanofibrous webs of OSL and cellulose triacetate (CT) were produced by electrospinning and the thickening ability of these in castor oil was verified. The morphology of electrospun OSL/CT nanostructures can be modulated by modifying the OSL:CT weight ratio and it is dependent on the intrinsic properties of the solution. Electrospun OSL/CT nanostructures were formed by filament-interconnected particles, BOAS, or well-developed uniform nanofiber. The linear viscoelastic response of the gel-like dispersions was qualitatively similar but SAOS functions increased with electrospun nanostructure concentration and CT proportion. The morphological characteristics of the electrospun nanostructures, i.e., the average fiber diameter significantly affect the viscous and viscoelastic properties of the resulting gel-like dispersions.

Acknowledgments

This work is a collaborative research of different projects: RTI2018- 096080-B-C21, RTI2018-096080-B-C22, PID2021-125637OB-I00, TED2021-132122B-C21 and ENE2017-85819-C2-2-R funded by MCIN/AEI/10.13039/501100011033 and by "ERDF A way of making Europe", SUSTEC-CM S2018/EMT-4348 project funded by Comunidad de Madrid. The authors gratefully acknowledge the aforementioned financial support. J.F.R.-V. additionally has received a Ph.D. Research Grant PRE2019-090632 from Spain's Ministry of Science and Innovation. The financial support is gratefully acknowledged.

References

[1] A. Susmozas, R. Martín-Sampedro, D. Ibarra, M.E. Eugenio, R. Iglesias, P. Manzanares, A.D. Moreno, Process Strategies for the Transition of 1G to Advanced Bioethanol Production, Processes. 8 (2020) 1310. https://doi.org/10.3390/pr8101310.

[2] A. Arevalo-Gallegos, Z. Ahmad, M. Asgher, R. Parra-Saldivar, H.M.N. Iqbal, Lignocellulose: A sustainable material to produce value-added products with a zero waste approach—A review, Int. J. Biol. Macromol. 99 (2017) 308–318. https://doi.org/10.1016/j.ijbiomac.2017.02.097.

[3] https://www.fao.org/faostat/en/#data/QCL.

[4] P. Doménech, A. Duque, I. Higueras, R. Iglesias, P. Manzanares, Biorefinery of the Olive Tree—Production of Sugars from Enzymatic Hydrolysis of Olive Stone Pretreated by Alkaline Extrusion, Energies. 13 (2020) 4517. https://doi.org/10.3390/en13174517.

[5] C. Padilla-Rascón, E. Ruiz, I. Romero, E. Castro, J.M. Oliva, I. Ballesteros, P. Manzanares, Valorisation of olive stone by-product for sugar production using a sequential acid/steam explosion pretreatment, Ind. Crops Prod. 148 (2020) 112279. https://doi.org/10.1016/j.indcrop.2020.112279.

[6] EU Dir. 2018/2001 Eur. Parliam. Counc. 11 December 2018 Promot. Use Energy from Renew. Sources, Eur. Parliam. Counc. Eur. Union Brussels, Belgium, 2018, n.d. https://doi.org/https://eur-lex.europa.eu/eli/dir/2018/2001/oj.

[7] T. Raj, K. Chandrasekhar, A. Naresh Kumar, J. Rajesh Banu, J.-J. Yoon, S. Kant Bhatia, Y.-H. Yang, S. Varjani, S.-H. Kim, Recent advances in commercial biorefineries for lignocellulosic ethanol production: Current status, challenges and future perspectives, Bioresour. Technol. 344 (2022) 126292. https://doi.org/10.1016/j.biortech.2021.126292.

[8] A.J. Ragauskas, G.T. Beckham, M.J. Biddy, R. Chandra, F. Chen, M.F. Davis, B.H. Davison, R.A. Dixon, P. Gilna, M. Keller, P. Langan, A.K. Naskar, J.N. Saddler, T.J.

Tschaplinski, G.A. Tuskan, C.E. Wyman, Lignin Valorization: Improving Lignin Processing in the Biorefinery, Science (80-.). 344 (2014). https://doi.org/10.1126/science.1246843.

[9] J. Ralph, K. Lundquist, G. Brunow, F. Lu, H. Kim, P.F. Schatz, J.M. Marita, R.D. Hatfield, S.A. Ralph, J.H. Christensen, W. Boerjan, Lignins: Natural polymers from oxidative coupling of 4-hydroxyphenyl- propanoids, Phytochem. Rev. 3 (2004) 29–60. https://doi.org/10.1023/B:PHYT.0000047809.65444.a4.

[10] P. Azadi, O.R. Inderwildi, R. Farnood, D.A. King, Liquid fuels, hydrogen and chemicals from lignin: A critical review, Renew. Sustain. Energy Rev. 21 (2013) 506–523. https://doi.org/10.1016/j.rser.2012.12.022.

[11] A.M. Borrero-López, F.J. Santiago-Medina, C. Valencia, M.E. Eugenio, R. Martin-Sampedro, J.M. Franco, Valorization of Kraft Lignin as Thickener in Castor Oil for Lubricant Applications, J. Renew. Mater. 6 (2018) 347–361. https://doi.org/10.7569/JRM.2017.634160.

[12] T. Shahzadi, S. Mehmood, M. Irshad, Z. Anwar, A. Afroz, N. Zeeshan, U. Rashid, K. Sughra, Advances in lignocellulosic biotechnology: A brief review on lignocellulosic biomass and cellulases, Adv. Biosci. Biotechnol. 05 (2014) 246–251. https://doi.org/10.4236/abb.2014.53031.

[13] N. Núñez, J.E. Martín-Alfonso, C. Valencia, M.C. Sánchez, J.M. Franco, Rheology of new green lubricating grease formulations containing cellulose pulp and its methylated derivative as thickener agents, Ind. Crops Prod. 37 (2012) 500–507. https://doi.org/10.1016/j.indcrop.2011.07.027.

[14] R. Gallego, J.F. Arteaga, C. Valencia, J.M. Franco, Rheology and thermal degradation of isocyanate-functionalized methyl cellulose-based oleogels, Carbohydr. Polym. 98 (2013) 152–160. https://doi.org/10.1016/j.carbpol.2013.04.104.

[15] M. Trejo-Cáceres, M.C. Sánchez, J.E. Martín-Alfonso, Impact of acetylation process of kraft lignin in development of environment-friendly semisolid lubricants, Int. J. Biol. Macromol. 227 (2023) 673–684. https://doi.org/10.1016/j.ijbiomac.2022.12.096.

[16] T.M. Panchal, A. Patel, D.D. Chauhan, M. Thomas, J. V. Patel, A methodological review on bio-lubricants from vegetable oil based resources, Renew. Sustain. Energy Rev. 70 (2017) 65–70. https://doi.org/10.1016/j.rser.2016.11.105.

[17] A.Z. Syahir, N.W.M. Zulkifli, H.H. Masjuki, M.A. Kalam, A. Alabdulkarem, M. Gulzar, L.S. Khuong, M.H. Harith, A review on bio-based lubricants and their applications, J. Clean. Prod. 168 (2017) 997–1016. https://doi.org/10.1016/j.jclepro.2017.09.106.

[18] A.M. Borrero-López, R. Martín-Sampedro, D. Ibarra, C. Valencia, M.E. Eugenio, J.M. Franco, Evaluation of lignin-enriched side-streams from different biomass conversion processes as thickeners in bio-lubricant formulations, Int. J. Biol. Macromol. 162 (2020) 1398–1413. https://doi.org/10.1016/j.ijbiomac.2020.07.292.

[19] A.M. Borrero-López, C. Valencia, J.M. Franco, Lignocellulosic Materials for the Production of Biofuels, Biochemicals and Biomaterials and Applications of Lignocellulose-Based Polyurethanes: A Review, Polymers (Basel). 14 (2022) 881. https://doi.org/10.3390/polym14050881.

[20] E. Cortés-Triviño, C. Valencia, M.A. Delgado, J.M. Franco, Rheology of epoxidized cellulose pulp gel-like dispersions in castor oil: Influence of epoxidation degree and the epoxide chemical structure, Carbohydr. Polym. 199 (2018) 563–571. https://doi.org/10.1016/j.carbpol.2018.07.058.

[21] E. Cortés-Triviño, C. Valencia, J.M. Franco, Influence of epoxidation conditions on the rheological properties of gel-like dispersions of epoxidized kraft lignin in castor oil, Holzforschung. 71 (2017) 777–784. https://doi.org/10.1515/hf-2017-0012.

[22] J.F. Rubio-Valle, M.C. Sánchez, C. Valencia, J.E. Martín-Alfonso, J.M. Franco,

Electrohydrodynamic Processing of PVP-Doped Kraft Lignin Micro- and Nano-Structures and Application of Electrospun Nanofiber Templates to Produce Oleogels, Polymers (Basel). 13 (2021) 2206. https://doi.org/10.3390/polym13132206.

[23] J.F. Rubio-Valle, C. Valencia, M. Sánchez, J.E. Martín-Alfonso, J.M. Franco, Oil structuring properties of electrospun Kraft lignin/cellulose acetate nanofibers for lubricating applications: influence of lignin source and lignin/cellulose acetate ratio, Cellulose. 30 (2023) 1553–1566. https://doi.org/10.1007/s10570-022-04963-2.

[24] M. Borrego, J.E. Martín-Alfonso, C. Valencia, M.C. Sánchez, J.M. Franco, Impact of the Morphology of Electrospun Lignin/Ethylcellulose Nanostructures on Their Capacity to Thicken Castor Oil, Polymers (Basel). 14 (2022) 4741. https://doi.org/10.3390/polym14214741.

[25] J.F. Rubio-Valle, M. Jiménez-Rosado, V. Perez-Puyana, A. Guerrero, A. Romero, Electrospun nanofibres with antimicrobial activities, in: Antimicrob. Text. from Nat. Resour., Elsevier, 2021: pp. 589–618. https://doi.org/10.1016/B978-0-12-821485-5.00020-2.

[26] I. Dallmeyer, F. Ko, J.F. Kadla, Correlation of Elongational Fluid Properties to Fiber Diameter in Electrospinning of Softwood Kraft Lignin Solutions, Ind. Eng. Chem. Res. 53 (2014) 2697–2705. https://doi.org/10.1021/ie403724y.

[27] M. Borrego, J.E. Martín-Alfonso, M.C. Sánchez, C. Valencia, J.M. Franco, Electrospun lignin-PVP nanofibers and their ability for structuring oil, Int. J. Biol. Macromol. 180 (2021) 212–221. https://doi.org/10.1016/j.ijbiomac.2021.03.069.

[28] I. Dallmeyer, F. Ko, J.F. Kadla, Electrospinning of Technical Lignins for the Production of Fibrous Networks, J. Wood Chem. Technol. 30 (2010) 315–329. https://doi.org/10.1080/02773813.2010.527782.

[29] I. Dallmeyer, L.T. Lin, Y. Li, F. Ko, J.F. Kadla, Preparation and Characterization of

675 Interconnected, Kraft Lignin-Based Carbon Fibrous Materials by Electrospinning,
676 Macromol. Mater. Eng. 299 (2014) 540–551. https://doi.org/10.1002/mame.201300148.
677 [30] L. García-Fuentevilla, J.F. Rubio-Valle, R. Martín-Sampedro, C. Valencia, M.E.
678 Eugenio, D. Ibarra, Different Kraft lignin sources for electrospun nanostructures
679 production: Influence of chemical structure and composition, Int. J. Biol. Macromol. 214
680 (2022) 554–567. https://doi.org/10.1016/j.ijbiomac.2022.06.121.
681 [31] D. Ibarra, L. García-Fuentevilla, J.F. Rubio-Valle, R. Martín-Sampedro, C. Valencia,
682 M.E. Eugenio, Kraft lignins from different poplar genotypes obtained by selective acid
683 precipitation and their use for the production of electrospun nanostructures, React. Funct.
684 Polym. 191 (2023) 105685. https://doi.org/10.1016/j.reactfunctpolym.2023.105685.
685 [32] M.A. Teixeira, M.C. Paiva, M.T.P. Amorim, H.P. Felgueiras, Electrospun
686 nanocomposites containing cellulose and its derivatives modified with specialized
687 biomolecules for an enhanced wound healing, Nanomaterials. 10 (2020).
688 https://doi.org/10.3390/nano10030557.
689 [33] P. Sánchez-Cid, J.F. Rubio-Valle, M. Jiménez-Rosado, V. Pérez-Puyana, A. Romero,
690 Effect of Solution Properties in the Development of Cellulose Derivative Nanostructures
691 Processed via Electrospinning, Polymers (Basel). 14 (2022) 665.
692 https://doi.org/10.3390/polym14040665.
693 [34] R. Konwarh, N. Karak, M. Misra, Electrospun cellulose acetate nanofibers: The present
694 status and gamut of biotechnological applications, Biotechnol. Adv. 31 (2013) 421–437.
695 https://doi.org/10.1016/j.biotechadv.2013.01.002.
696 [35] L.A. Quinchia, M.A. Delgado, C. Valencia, J.M. Franco, C. Gallegos, Viscosity
697 modification of different vegetable oils with EVA copolymer for lubricant applications,
698 Ind. Crops Prod. 32 (2010) 607–612. https://doi.org/10.1016/j.indcrop.2010.07.011.
699 [36] J.B. Sluiter, R.O. Ruiz, C.J. Scarlata, A.D. Sluiter, D.W. Templeton, Compositional

Analysis of Lignocellulosic Feedstocks. 1. Review and Description of Methods, J. Agric. Food Chem. 58 (2010) 9043–9053. https://doi.org/10.1021/jf1008023.

[37] L. Jiménez-López, R. Martín-Sampedro, M.E. Eugenio, J.I. Santos, H. Sixto, I. Cañellas, D. Ibarra, Co-production of soluble sugars and lignin from short rotation white poplar and black locust crops, Wood Sci. Technol. 54 (2020) 1617–1643. https://doi.org/10.1007/s00226-020-01217-x.

[38] J.F. Rubio-Valle, M.C. Sánchez, C. Valencia, J.E. Martín-Alfonso, J.M. Franco, Production of lignin/cellulose acetate fiber-bead structures by electrospinning and exploration of their potential as green structuring agents for vegetable lubricating oils, Ind. Crops Prod. 188 (2022) 115579. https://doi.org/10.1016/j.indcrop.2022.115579.

[39] A.D. Moreno, L. Olsson, Pretreatment of Lignocellulosic Feedstocks, in: Extrem. Enzym. Process. Lignocellul. Feed. to Bioenergy, Springer International Publishing, Cham, 2017: pp. 31–52. https://doi.org/10.1007/978-3-319-54684-1_3.

[40] P. Alvira, M. Ballesteros, M.J. Negro, Progress on Enzymatic Saccharification Technologies for Biofuels Production, in: Biofuel Technol., Springer Berlin Heidelberg, Berlin, Heidelberg, 2013: pp. 145–169. https://doi.org/10.1007/978-3-642-34519-7_6.

[41] M.Á.B. Alcántara, J. Dobruchowska, P. Azadi, B.D. García, F.P. Molina-Heredia, F.M. Reyes-Sosa, Recalcitrant carbohydrates after enzymatic hydrolysis of pretreated lignocellulosic biomass, Biotechnol. Biofuels. 9 (2016) 207. https://doi.org/10.1186/s13068-016-0629-4.

[42] J.I. Santos, R. Martín-Sampedro, Ú. Fillat, J.M. Oliva, M.J. Negro, M. Ballesteros, M.E. Eugenio, D. Ibarra, Evaluating Lignin-Rich Residues from Biochemical Ethanol Production of Wheat Straw and Olive Tree Pruning by FTIR and 2D-NMR, Int. J. Polym. Sci. 2015 (2015) 1–11. https://doi.org/10.1155/2015/314891.

[43] J.I. Santos, Ú. Fillat, R. Martín-Sampedro, M.E. Eugenio, M.J. Negro, I. Ballesteros, A.

Rodríguez, D. Ibarra, Evaluation of lignins from side-streams generated in an olive tree pruning-based biorefinery: Bioethanol production and alkaline pulping, Int. J. Biol. Macromol. 105 (2017) 238–251. https://doi.org/10.1016/j.ijbiomac.2017.07.030.

[44] A.M. Borrero-López, C. Valencia, D. Ibarra, I. Ballesteros, J.M. Franco, Lignin-enriched residues from bioethanol production: Chemical characterization, isocyanate functionalization and oil structuring properties, Int. J. Biol. Macromol. 195 (2022) 412–423. https://doi.org/10.1016/j.ijbiomac.2021.11.185.

[45] M. Alekhina, O. Ershova, A. Ebert, S. Heikkinen, H. Sixta, Softwood kraft lignin for value-added applications: Fractionation and structural characterization, Ind. Crops Prod. 66 (2015) 220–228. https://doi.org/10.1016/j.indcrop.2014.12.021.

[46] D. Ibarra, J.C. de. Río, A. Gutiérrez, I.M. Rodríguez, J. Romero, M.J. Martínez, Á.T. Martínez, Isolation of high-purity residual lignins from eucalypt paper pulps by cellulase and proteinase treatments followed by solvent extraction, Enzyme Microb. Technol. 35 (2004) 173–181. https://doi.org/10.1016/j.enzmictec.2004.04.002.

[47] J. Li, G. Henriksson, G. Gellerstedt, Lignin depolymerization/repolymerization and its critical role for delignification of aspen wood by steam explosion, Bioresour. Technol. 98 (2007) 3061–3068. https://doi.org/10.1016/j.biortech.2006.10.018.

[48] R. Samuel, M. Foston, N. Jaing, S. Cao, L. Allison, M. Studer, C. Wyman, A.J. Ragauskas, HSQC (heteronuclear single quantum coherence) 13C–1H correlation spectra of whole biomass in perdeuterated pyridinium chloride–DMSO system: An effective tool for evaluating pretreatment, Fuel. 90 (2011) 2836–2842. https://doi.org/10.1016/j.fuel.2011.04.021.

[49] S. Heikkinen, M.M. Toikka, P.T. Karhunen, I.A. Kilpeläinen, Quantitative 2D HSQC (Q-HSQC) via Suppression of J -Dependence of Polarization Transfer in NMR Spectroscopy: Application to Wood Lignin, J. Am. Chem. Soc. 125 (2003) 4362–4367.

https://doi.org/10.1021/ja029035k.

[50] H. Wang, Z. Liu, L. Hui, L. Ma, X. Zheng, J. Li, Y. Zhang, Understanding the structural changes of lignin in poplar following steam explosion pretreatment, Holzforschung. 74 (2020) 275–285. https://doi.org/10.1515/hf-2019-0087.

[51] J. Rencoret, A. Gutiérrez, E. Castro, J.C. del Río, Structural characteristics of lignin in pruning residues of olive tree (Olea europaea L.), Holzforschung. 73 (2018) 25–34. https://doi.org/10.1515/hf-2018-0077.

[52] F. Araya, E. Troncoso, R.T. Mendonça, J. Freer, Condensed lignin structures and re-localization achieved at high severities in autohydrolysis of Eucalyptus globulus wood and their relationship with cellulose accessibility, Biotechnol. Bioeng. 112 (2015) 1783–1791. https://doi.org/10.1002/bit.25604.

[53] A. Lourenço, S. Araújo, J. Gominho, H. Pereira, D. Evtuguin, Structural changes in lignin of thermally treated eucalyptus wood, J. Wood Chem. Technol. 40 (2020) 258–268. https://doi.org/10.1080/02773813.2020.1769674.

[54] S.O. Prozil, D. V. Evtuguin, A.M.S. Silva, L.P.C. Lopes, Structural Characterization of Lignin from Grape Stalks (Vitis vinifera L.), J. Agric. Food Chem. 62 (2014) 5420–5428. https://doi.org/10.1021/jf502267s.

[55] C. Padilla-Rascon, E. Ruiz, E. Castro, L.B. Roseiro, L.C. Duarte, F. Carvalheiro, Effective Production of Bioactive Phenolic Compounds from Olive Stones, in: 2nd Int. Electron. Conf. Foods - "Future Foods Food Technol. a Sustain. World," MDPI, Basel Switzerland, 2021: p. 70. https://doi.org/10.3390/Foods2021-10940.

[56] J. Rencoret, G. Marques, A. Gutiérrez, D. Ibarra, J. Li, G. Gellerstedt, J.I. Santos, J. Jiménez-Barbero, Á.T. Martínez, J.C. del Río, Structural characterization of milled wood lignins from different eucalypt species, Holzforschung. 62 (2008). https://doi.org/10.1515/HF.2008.096.

[57] M.E. Eugenio, R. Martín-Sampedro, J.I. Santos, B. Wicklein, D. Ibarra, Chemical, Thermal and Antioxidant Properties of Lignins Solubilized during Soda/AQ Pulping of Orange and Olive Tree Pruning Residues, Molecules. 26 (2021) 3819. https://doi.org/10.3390/molecules26133819.

[58] R. Martín-Sampedro, J.I. Santos, M.E. Eugenio, B. Wicklein, L. Jiménez-López, D. Ibarra, Chemical and thermal analysis of lignin streams from Robinia pseudoacacia L. generated during organosolv and acid hydrolysis pre-treatments and subsequent enzymatic hydrolysis, Int. J. Biol. Macromol. 140 (2019) 311–322. https://doi.org/10.1016/j.ijbiomac.2019.08.029.

[59] A. Tolbert, H. Akinosho, R. Khunsupat, A.K. Naskar, A.J. Ragauskas, Characterization and analysis of the molecular weight of lignin for biorefining studies, Biofuels, Bioprod. Biorefining. 8 (2014) 836–856. https://doi.org/10.1002/bbb.1500.

[60] M. Borrego, J.E. Martín-Alfonso, C. Valencia, M. del C. Sánchez Carrillo, J.M. Franco, Developing Electrospun Ethylcellulose Nanofibrous Webs: An Alternative Approach for Structuring Castor Oil, ACS Appl. Polym. Mater. 4 (2022) 7217–7227. https://doi.org/10.1021/acsapm.2c01090.

[61] N. Alwadani, N. Grishkewich, P. Fatehi, Surface and interface characteristics of hydrophobic lignin derivatives in solvents and films, Colloids Surfaces A Physicochem. Eng. Asp. 609 (2021) 125656. https://doi.org/10.1016/j.colsurfa.2020.125656.

[62] S. Kubo, J.F. Kadla, Hydrogen Bonding in Lignin: A Fourier Transform Infrared Model Compound Study, Biomacromolecules. 6 (2005) 2815–2821. https://doi.org/10.1021/bm050288q.

[63] M.A. Martín-Alfonso, J.F. Rubio-Valle, J.P. Hinestroza, J.E. Martín-Alfonso, Impact of Vegetable Oil Type on the Rheological and Tribological Behavior of Montmorillonite-Based Oleogels, Gels. 8 (2022) 504. https://doi.org/10.3390/gels8080504.

800 [64] R. Gallego, J.F. Arteaga, C. Valencia, M.J. Díaz, J.M. Franco, Gel-Like Dispersions of
801 HMDI-Cross-Linked Lignocellulosic Materials in Castor Oil: Toward Completely
802 Renewable Lubricating Grease Formulations, ACS Sustain. Chem. Eng. 3 (2015) 2130–
803 2141. https://doi.org/10.1021/acssuschemeng.5b00389.
804 [65] E. Cortés-Triviño, C. Valencia, M.A. Delgado, J.M. Franco, Thermo-rheological and
805 tribological properties of novel bio-lubricating greases thickened with epoxidized
806 lignocellulosic materials, J. Ind. Eng. Chem. 80 (2019) 626–632.
807 https://doi.org/10.1016/j.jiec.2019.08.052.
808 [66] R. Sánchez, C. Valencia, J.M. Franco, Rheological and Tribological Characterization of
809 a New Acylated Chitosan–Based Biodegradable Lubricating Grease: A Comparative
810 Study with Traditional Lithium and Calcium Greases, Tribol. Trans. 57 (2014) 445–454.
811 https://doi.org/10.1080/10402004.2014.883541.
812 [67] M.A. Delgado, C. Valencia, M.C. Sánchez, J.M. Franco, C. Gallegos,
813 Thermorheological behaviour of a lithium lubricating grease, Tribol. Lett. 23 (2006) 47–
814 54. https://doi.org/10.1007/s11249-006-9109-5.
815 [68] J.D. Ferry, Viscoelastic properties of polymers, 3rd ed., New York, 1980.
816
817

Highlights

- Valorization of lignin-rich residue from the bioethanol production of olive stones
- Lignin-rich residue presented the main inter-unit linkages and low S/G ratios
- Electrospinning of lignin-rich residue (OSL) and cellulose triacetate (CT)
- Castor oil structuring ability of electrospun OSL/CT nanostructures
- Rheological properties of gel-like dispersions tuned by OSL/CA weight ratio